Microstructure of high strength steel refined with intragranularly nucleated Widmanstätten ferrite

A. Ali and H. K. D. H. Bhadeshia

A method has been developed to refine the microstructure of clean, high strength martensitic steels by partitioning the austenite grain structure with intragranularly nucleated plates of Widmanstätten ferrite. The plates were induced to nucleate heterogeneously on oxide particles present in the steels, by first forming uniform, thin layers of inactive allotriomorphic ferrite at the austenite grain surfaces. This effectively removed the austenite grain boundaries as potential sites for the nucleation of Widmanstätten ferrite, which consequently nucleated intragranularly on impurity oxide particles. The intragranularly nucleated ferrite plates were found to radiate in many directions from each oxide particle, in a manner which subdivided the remaining austenite into fine blocks. Quenching after this partial transformation to allotriomorphic and Widmanstätten ferrite resulted in the martensitic decomposition of the blocks of residual austenite, leading to a significantly refined overall microstructure.

MST/1438

 Manuscript received 11 March 1991. *The authors are in the Department of Materials Science and Metallurgy, University of Cambridge/JRDC.*

Introduction

Microstructural observations have demonstrated that during cleavage failure, cracks propagate virtually undeviated across individual sheaves of bainite in low carbon, low alloy steels.[1] Similar results have been reported for low carbon, low alloy weld deposits, where qualitative evidence suggests that cleavage cracks propagate undeflected across packets of identically orientated bainite platelets, but have to reinitiate on encountering sheaf boundaries.[2] The size of cleavage facets obtained by brittle fracture was found to correlate well with the width of bainite sheaves, i.e. the packet size,[3] although there are other results which suggest that the unit crack path is somewhat larger than the packet size.[4,5] The unit crack path length is defined simply as the region within which crack propagation is approximately linear.[6,7] That the path length tends to be somewhat greater than the sheaf width may be associated with the possibility of adjacent bainite sheaves, which are different variants of the orientation relationship with austenite, still having their cleavage planes fairly parallel.[5] Thus, any discrepancy between the packet size and unit crack path length does not weaken the basic argument that having a set of parallel ferrite plates in identical orientation adversely affects toughness. Instead, it leads to a more general stipulation that groups of plates should not have a common cleavage plane.

The idea that a 'chaotic' microstructure (rather than one containing ferrite plates neatly arranged into packets) improves toughness is very prominent in the welding industry.[8–11] Hence, controlled quantities of specific types of non-metallic inclusion are tolerated in weld deposits, because they serve to stimulate the intragranular nucleation of ferrite platelets that radiate in many different directions from the inclusion nucleation sites. Such a microstructure in welds is denoted 'acicular ferrite', although it is now appreciated that acicular ferrite is only intragranularly nucleated bainite.[12] A propagating crack then has to traverse plates in many different crystallographic orientations. Non-metallic inclusions are otherwise regarded as harmful, since thay can often be responsible for initiating cleavage or void nucleation. Using the same reasoning, deliberate additions of titanium oxide particles have recently been made to wrought steels to induce intragranular nucleation of acicular ferrite.[13–17]

Similar phenomena are observed in quenched and tempered martensitic steel. Fractographic measurements indicate that the dominant microstructural feature in the process of cleavage fracture is the size of the martensite packet.[18] For heavily alloyed, ultrahigh strength steels, ausformed martensites have been demonstrated to have a more chaotic spatial and size distribution of plates when compared with directly quenched martensitic microstructures.[19] This is one reason why ausformed steels also have a higher level of strength without undue sacrifice of toughness. Tomita and Okabayashi[20,21] demonstrated improvements in the mechanical properties of martensitic steels when the austenite grain structure was first partitioned into smaller regions by partial transformation to bainite. The small quantity of grain boundary nucleated bainite sheaves effectively refined the austenite grains before martensitic transformation.

The purpose of the present work is to investigate an alternative method of achieving the same effect, suggested by recent research on Fe–C–Cr–Mo weld deposits.[22] Intragranular nucleation can be stimulated if the austenite grain boundaries are rendered ineffective as potential heterogeneous nucleation sites, by heat treatment to decorate them with thin layers of allotriomorphic ferrite (Fig. 1). For the technique to succeed, the allotriomorphic ferrite must not act as a substrate for either secondary Widmanstätten ferrite or bainite, since both of these are in the form of undesirable packets of parallel platelets and, indeed, consume austenite, which should be preserved for intragranularly nucleated transformation products. The allotriomorphic ferrite can be rendered innocuous if austenite stabilising elements partition during its growth.[22] This method of stimulating intragranular nucleation is particularly relevant in the context of high strength steels, because unlike weld deposits, cleanness is essential to achieve adequate toughness; thus, the number of oxide particles present must be kept to a minimum. It is their high strength which makes the steels much more susceptible to non-metallic inclusions as fracture initiators. The experiments reported here were consequently carried out using high purity steels, with the aim of producing a microstructure in which the packets of martensite could be refined by the presence of intragranularly nucleated Widmanstätten ferrite.

Experimental techniques

ALLOY PREPARATION

The alloys used were made as 20 kg vacuum induction melts using high purity base materials. The ingots were

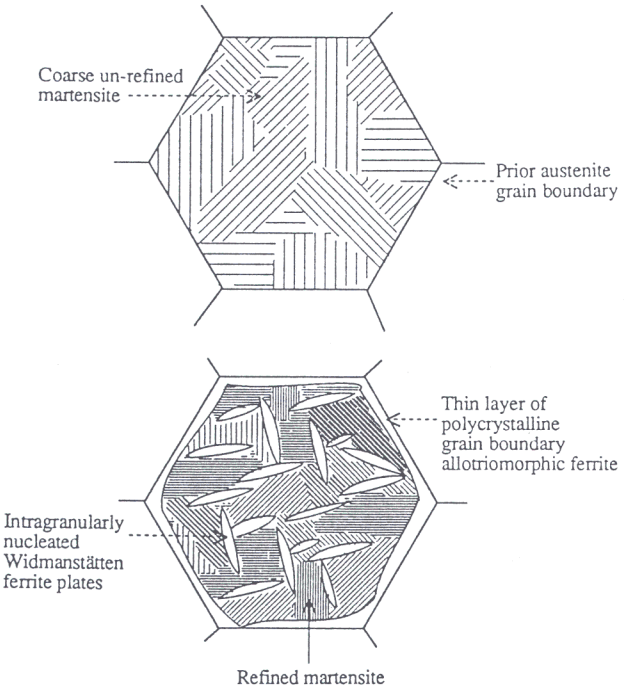

1 Schematic diagram of proposed method of refining martensitic microstructure with intragranularly nucleated plates of Widmanstätten ferrite

forged and hot rolled to 10 mm dia. rod, then hot swaged down to 6 mm dia. rod. After removing 2 mm from the surface by machining, the rods were cold swaged down to 3 mm dia., sealed in quartz tubes containing pure argon, and homogenised at 1250°C for 3 days. The chemical compositions of the alloys used (designated A1 and A2) are given in Table 1. The silicon concentration of the alloys is relatively high at about 2%, which retards tempering by impeding the precipitation of cementite.[23,24] As is discussed below, the overall chemistry of the alloys is ideal for the present work, since the C-curves for allotriomorphic and Widmanstätten ferrite on the time–temperature–transformation (TTT) diagrams are well separated. Silicon also prevents interference from the pearlite reaction. An essential difference between the alloys is that alloy A2 contains molybdenum, which has a retarding effect on transformation kinetics.

HEAT TREATMENTS (Table 2)

The heat treatments, which were carried out using electrical resistance heated furnaces, were designed to study the effect of isothermal transformation temperature and time and austenitisation temperature (*see* Fig. 2). The samples were in turn sealed in a quartz tube under a partial pressure (at ambient temperature) of pure argon and subjected to the austenitising heat treatments. For isothermal transformation, the quartz tubes were carefully fractured and the samples were immersed in a fluidised bed, maintained at the reaction temperature (controlled to ± 3 K), and reacted for various times before quenching into iced brine.

The calculated transformation temperatures of alloys A1 and A2 are given in Table 3.

Table 1 Chemical compositions of alloys used, wt-%

Code used	C	Si	Mn	Mo	Al	Ti	O
A1	0·22	2·07	3·00	...	0·011	0·004	0·0035
A2	0·22	2·05	3·07	0·70	0·005	0·004	0·0057

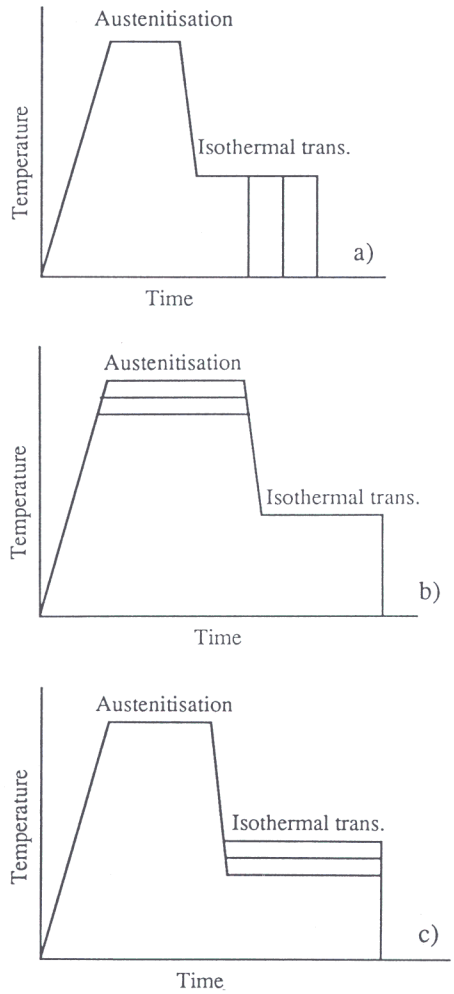

a variation of isothermal transformation time; *b* variation of austenitisation temperature; *c* variation of isothermal transformation temperature

2 Schematic diagrams of heat treatments used

MICROSCOPY AND MICROANALYSIS

Optical microscopy was carried out on specimens etched using a 2% nital solution. Thin foil specimens were prepared for transmission electron microscopy (TEM) from discs of 0·25 mm thickness sliced from the heat treated samples. The discs were thinned to about 0·04 mm by abrasion on 1200 grade SiC emery paper, then electropolished using a twin jet Fischione unit. The electrolyte consisted of a mixture of 5% perchloric acid, 25% glycerol, and 70% ethanol and was used at ambient temperature and 65 V polishing potential. The samples were examined on a Philips EM400T TEM operated at 120 kV, fitted with a Link 860 energy dispersive X-ray (EDX) microanalysis system. Standard thin foil correction programs were used to compensate for X-ray detection efficiency and absorption. For microanalytical purposes, the specimens were tilted 35° towards the detector.

Results and discussion

THEORETICAL ANALYSIS OF TRANSFORMATION CHARACTERISTICS

It has been found that Widmanstätten ferrite can in practice nucleate at a detectable rate when[26]

$$G_{max} \leqslant \Delta G_N \quad \ldots \quad (1)$$

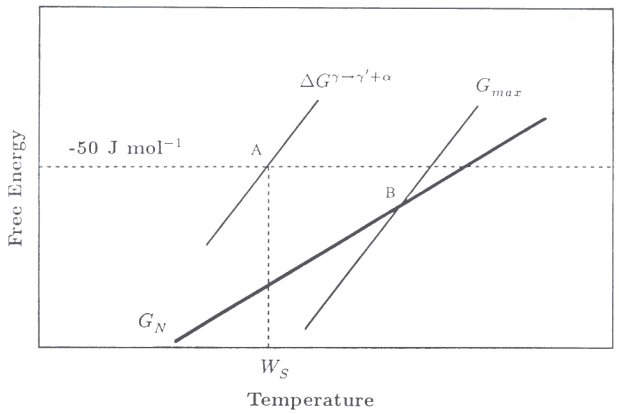

3 Schematic diagram of thermodynamic conditions for calculation of W_s temperature: G_N curve is common to all steels, whereas other curves are dependent on specific steel composition

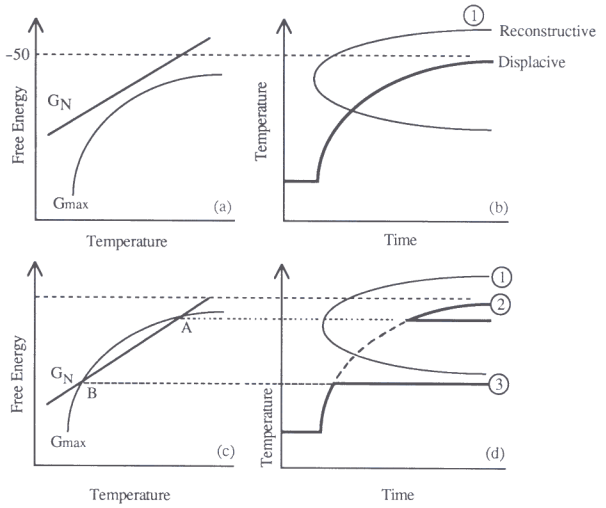

a–b conventional situation giving one displacive C-curve; *c–d* double intersection with displacive C-curve now separated into two segments Widmanstätten ferrite at high temperature (2) and bainite at low temperature (3)

4 Schematic diagram illustrating how double intersection of G_{max} curve with nucleation function G_N leads to splitting of displacive C-curve into two regions for separate formation of Widmanstätten ferrite and bainite

where G_{max} is the free energy change during nucleation (assuming that the nucleus adopts a composition that maximises this change) and G_N is a nucleation function (linear with temperature and common to all steels) representing the free energy change which must be exceeded before Widmanstätten ferrite can form at a detectable rate. In addition to this condition, growth should also be thermodynamically possible, which leads to the further criterion that the free energy change for growth $\Delta G^{\gamma\rightarrow\gamma'+\alpha}$ should exceed the stored energy of Widmanstätten ferrite

$$\Delta G^{\gamma\rightarrow\gamma'+\alpha} < -50 \text{ J mol}^{-1} \quad \ldots\ldots\ldots \quad (2)$$

Since the nucleation of bainite and Widmanstätten ferrite is described by the same function G_N, the nucleus is assumed to develop into bainite if the driving force for growth is sufficient to permit its diffusionless growth. Thus, bainite and Widmanstätten ferrite are usually represented by the same C-curve on the TTT diagram, with Widmanstätten ferrite forming between the Widmanstätten ferrite start W_s and bainite start B_s temperatures and bainite forming below B_s.* These concepts have been reported previously[26] and are shown here schematically in Fig. 3.

The aim was to induce the intragranular nucleation of a small volume fraction of Widmanstätten ferrite plates, in such a way that the plates do not grow in parallel formations. Nucleation on inclusions can achieve this because their submicrometre size cannot, in general, support the formation of more than one plate (although autocatalysis[30] can stimulate the formation of other plates in close proximity). There is not likely to be an opportunity for particle nucleation if the austenite grain boundary nucleation sites are active, since they are known[31] to be more effective nucleants, so that transformation originating from the grain surfaces can swamp any intragranular events. Grain boundary nucleated (i.e. secondary) Widmanstätten ferrite also has the unfortunate tendency to grow in packets of parallel plates. The boundaries can be rendered ineffective by heat treatment to decorate them with uniform, thin layers of allotriomorphic ferrite[22] which, by partitioning of austenite stabilising elements into the surrounding matrix, can be prevented from acting as substrates for the growth of secondary Widmanstätten ferrite. The steel utilised must therefore be very sluggish in its transformation to allotriomorphic ferrite.

High strength steels are in this respect eminently suitable, because they are usually heavily alloyed to improve hardenability. A less well known effect, first predicted theoretically in Ref. 29, is that the alloying leads to splitting

Table 2 Heat treatment schedules used for metallographic measurements

Identification	Heat treatment
Alloy A1	
1	1100°C/15 min + 680°C/264 h, WQ
2	680°C/600 h, WQ
3	700°C/ 53 h, WQ
4	700°C/100 h, WQ
5	700°C/144 h, WQ
6	700°C/216 h, WQ
7	720°C/120 h, WQ
8	720°C/346 h, WQ
9	740°C/240 h, WQ
10	1100°C/30 min + 680°C/264 h, WQ
11	700°C/264 h, WQ
12	720°C/264 h, WQ
13	740°C/264 h, WQ
14	1300°C/15 min + 680°C/264 h, WQ
15	740°C/264 h, WQ
Alloy A2	
1	1100°C/15 min + 680°C/600 h, WQ
2	700°C/600 h, WQ
3	720°C/240 h, WQ
4	740°C/240 h, WQ
5	1100°C/30 min + 680°C/264 h, WQ
6	700°C/264 h, WQ
7	720°C/264 h, WQ
8	740°C/264 h, WQ
9	1300°C/15 min + 680°C/264 h, WQ
10	740°C/264 h, WQ

WQ water quench.

* The TTT diagram can be considered to consist of two C-curves, that at higher temperatures representing reconstructive transformation, such as allotriomorphic ferrite and pearlite, and the other, extending to lower temperatures, for displacive reactions such as Widmanstätten ferrite and bainite.[29]

Table 3 Transformation temperatures calculated as in Refs. 25–28

Alloy	Ae_3	Ae_3	W_s	B_s	M_s
A1	812	773	700	477	338
A2	818	777	700	469	324

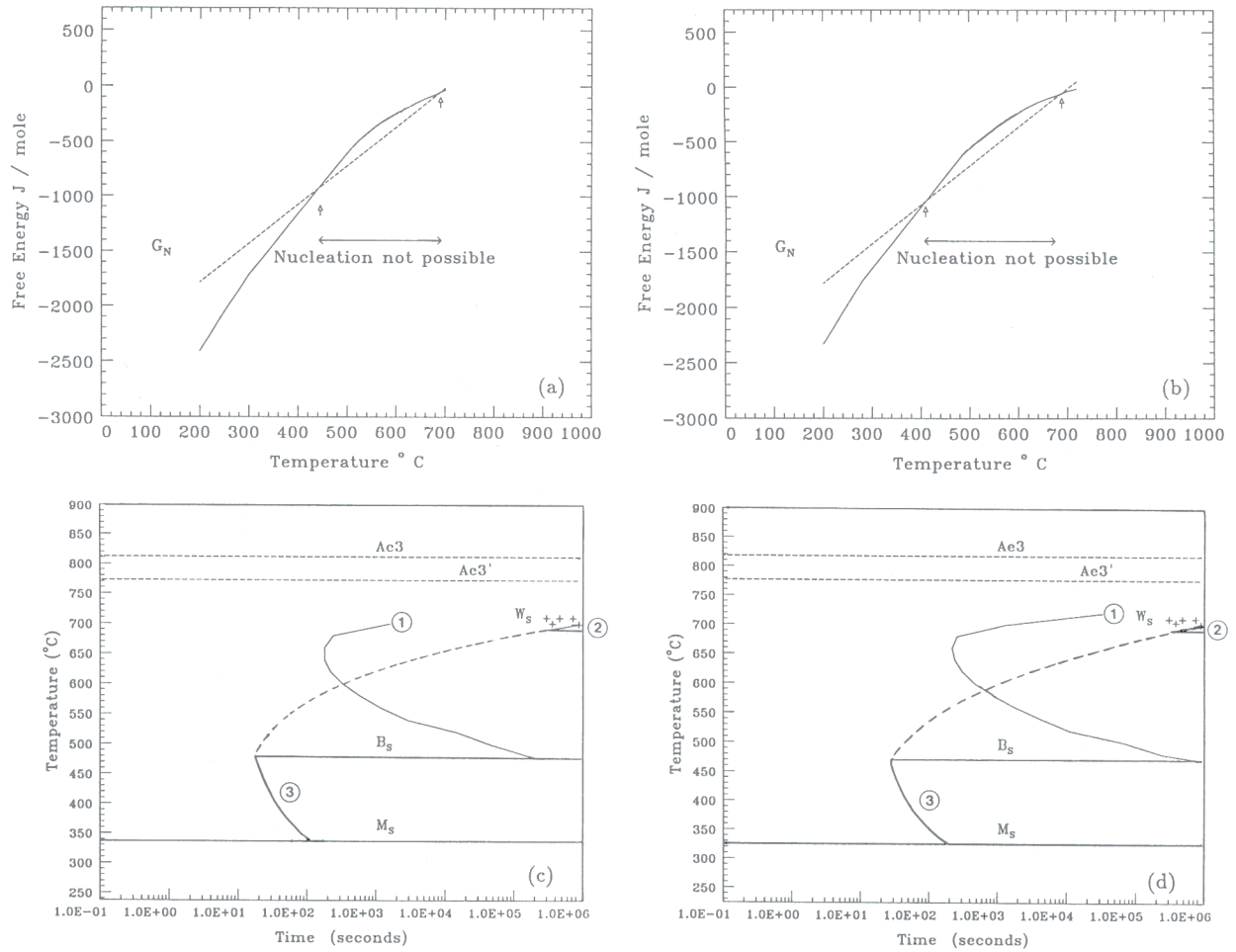

5 *a, b* **Calculated thermodynamic functions for two steels used in present work;** *c, d* **corresponding calculated TTT diagrams, with each diagram containing three C-curves (tiny Widmanstätten ferrite curves and bainite curves in** *c* **and** *d* **are connected by broken line intended to indicate how diagram would have appeared if G_{max} function intersected G_N at higher temperature only)**

of the displacive C-curve of the TTT diagram into separate Widmanstätten ferrite and bainite curves. The G_{max} function is significantly curved at high temperatures, so that, in principle, it can intersect the G_N line at two points (Fig. 4). Widmanstätten ferrite can then form at elevated temperatures, above the upper intersection temperature, and bainite can form at temperatures below the lower intersection (assuming that its growth is thermodynamically possible).

The steels used in the present study exhibit precisely this type of behaviour as illustrated in the calculated diagrams presented in Fig. 5. Alloys A1 and A2 were subjected to various heat treatments (*see* Table 2) that were designed to take advantage of the form of the TTT diagram, which indicates that allotriomorphic ferrite forms much before the onset of Widmanstätten ferrite, although the latter forms over a very narrow temperature range after prolonged heat treatment. They were also intended to provide further verification of the theory for Widmanstätten ferrite nucleation and growth.

METALLOGRAPHIC CONFIRMATION OF PREDICTED EFFECT

The metallographic results were examined to confirm that the heat treatment had led first to the growth of polycrystalline layers of allotriomorphic ferrite at the austenite grain surfaces, followed, after a time lag, by intragranular nucleation and growth of Widmanstätten ferrite. The most extensive data were collected for alloy A1, which is discussed first. It can be seen in Fig. 6 that the first transformation product is the allotriomorphic ferrite layers, although their coverage of the austenite grain surfaces is, at least during the initial stages of transformation, rather variable (Figs. 6*a* and 6*b*). As the isothermal heat treatment period was increased, the austenite grain boundaries became almost completely decorated with allotriomorphic ferrite. The first 6 days (144 h) of the heat treatment at 700°C were taken in forming the allotriomorphic layers; this period was followed by the profuse precipitation of intragranularly nucleated Widmanstätten ferrite. With very few exceptions (Fig. 6*d*), the allotriomorphs themselves did not appear to stimulate the growth of secondary Widmanstätten ferrite plates. There are two possible reasons why the allotriomorphic ferrite did not degenerate into Widmanstätten ferrite. First, although all allotriomorphs probably nucleate with an orientation relationship (which is within the 'Bain region'[32]) with at least one austenite grain,[33–35] selective growth along other grains can lead to a final microstructure in which most allotriomorphs are randomly orientated with respect to the adjacent austenite. The allotriomorphs cannot then develop into Widmanstätten ferrite, which, because of its displacive growth mechanism, is *always* related to its parent austenite with an orientation within the Bain region. Second, any partitioning of solute into the adjacent austenite during growth of the allotriomorphs can stabilise the austenite to displacive transformation.[35] Although the crystallographic aspects require further investigation to establish quantitatively, the appearance of well defined,

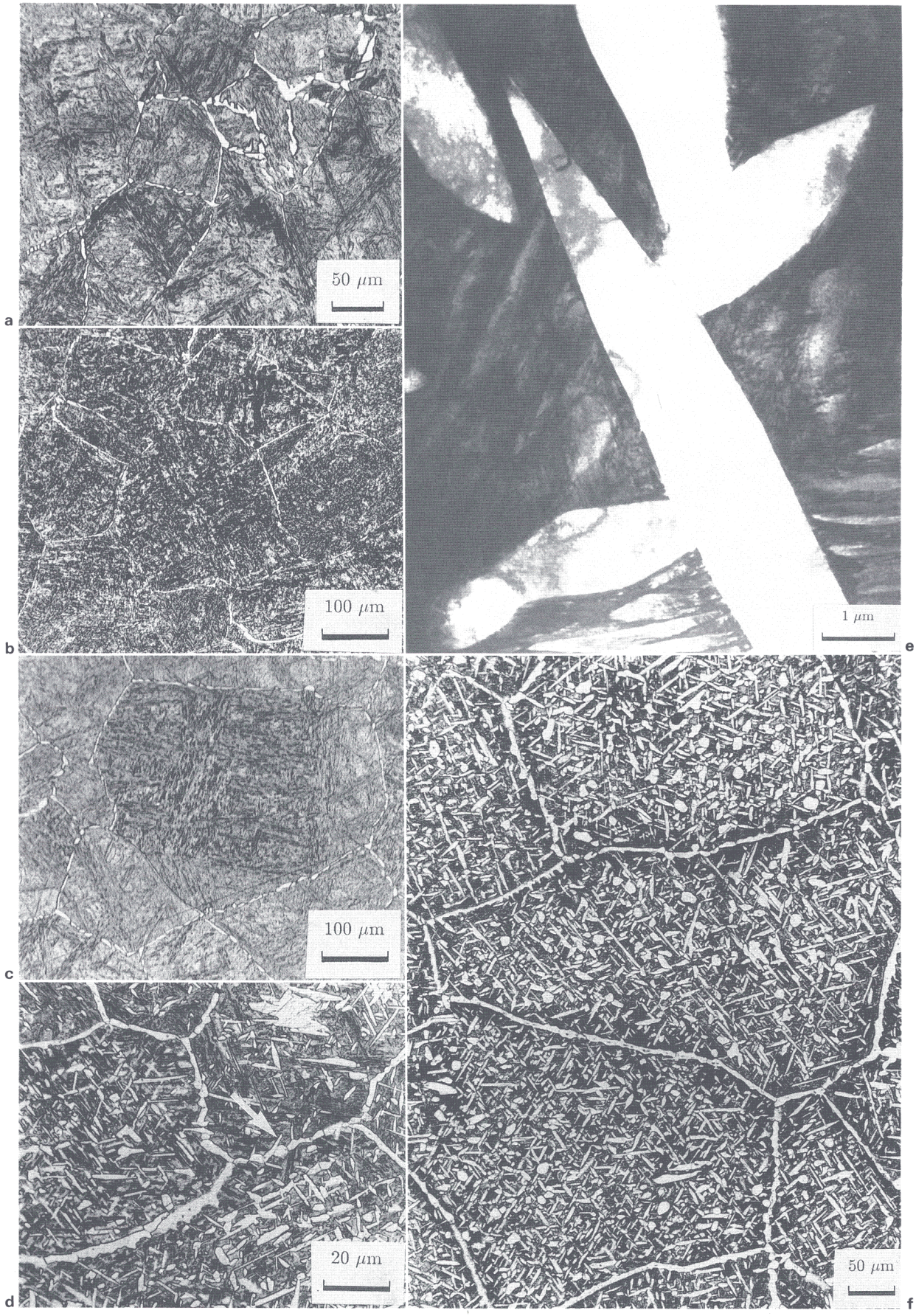

a 53 h (A1/3); *b* 100 h (A1/4); *c* 144 h (A1/5); *d* 216 h (A1/6 – arrow indicates secondary Widmanstätten ferrite plate); *e* 346 h (A1/8) intragranularly nucleated Widmanstätten ferrite; *f* larger field of view of microstructure of *d*, illustrating precipitate free zones in vicinity of allotriomorphic ferrite/austenite interfaces
a–d, f optical micrographs; *e* TEM

6 Alloy A1 after isothermal transformation at 700°C for various times

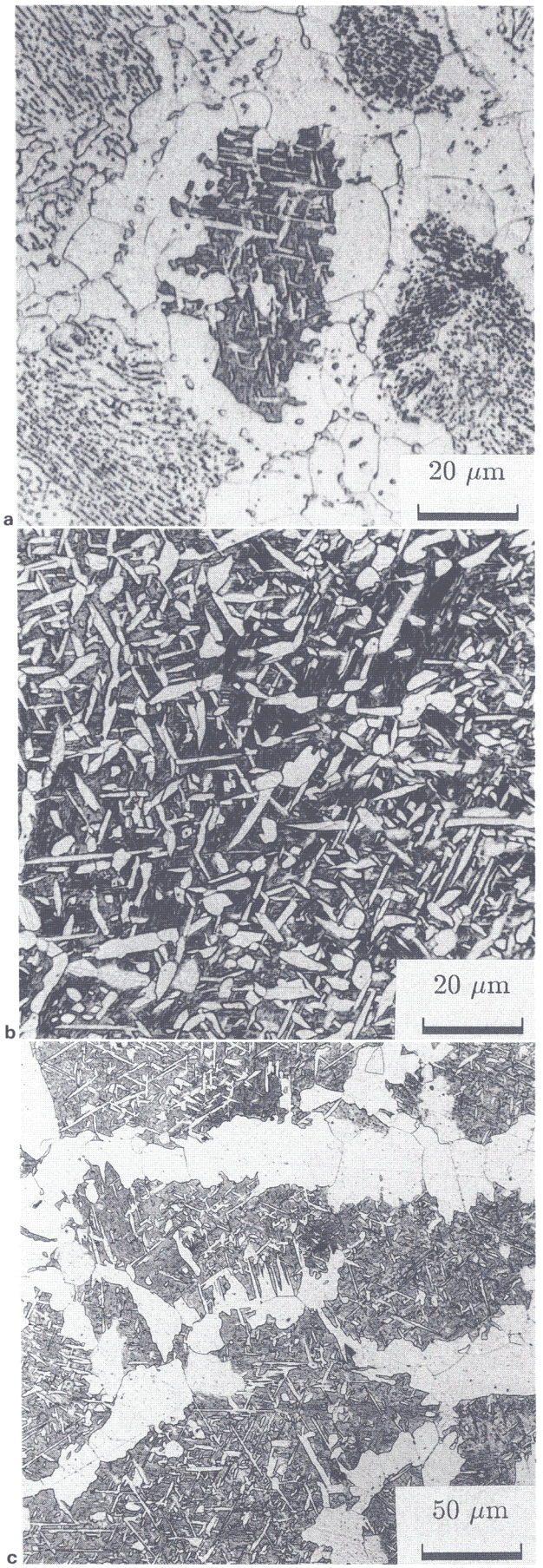

a 680°C/264 h (A1/1); *b* 720°C/346 h (A1/8); *c* 740°C/264 h (A1/13)

7 Optical micrographs of alloy A1 after various isothermal transformation treatments

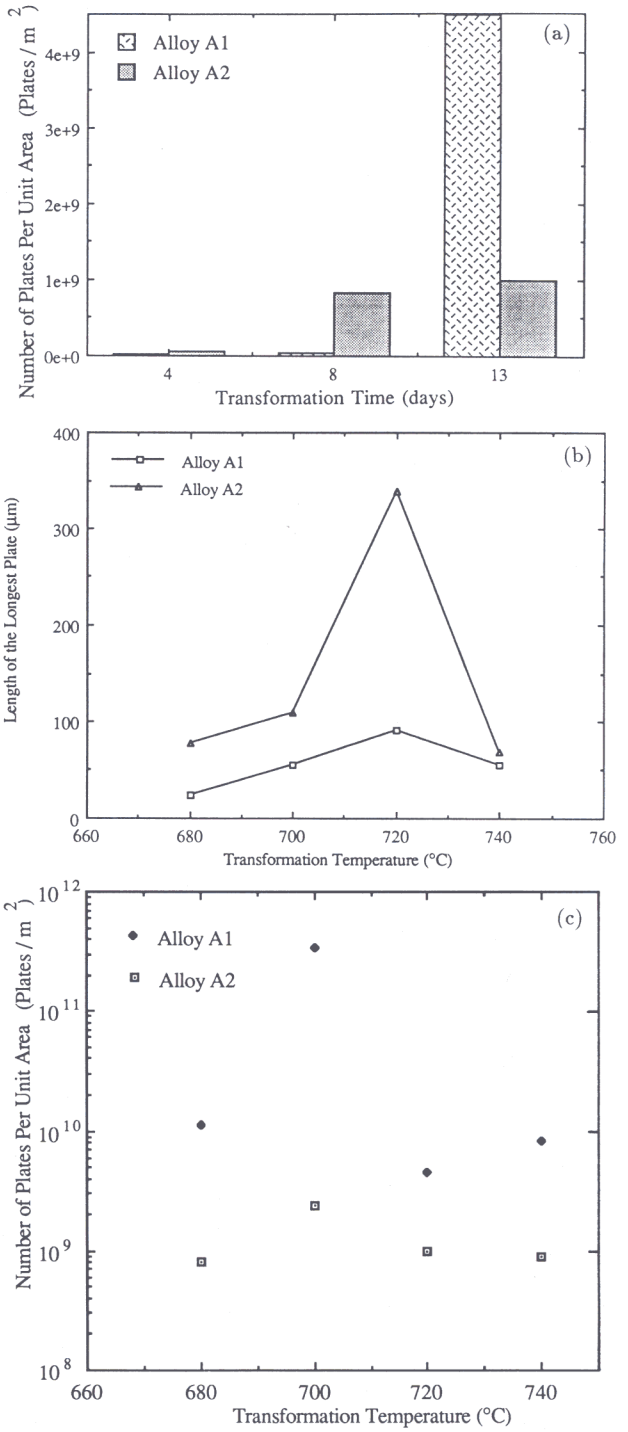

a histogram showing number of Widmanstätten ferrite plates per unit area counted on metallographic samples observed using optical microscopy at magnification of ×100, as function of time at isothermal transformation temperature of 720°C; *b* length of longest plate observed on random section as function of isothermal transformation temperature after holding at temperature for 264 h; *c* number of plates per unit area as function of transformation temperature after holding at temperature for 264 h

8 Results of metallographic measurements for alloys A1 and A2

precipitate free zones in the austenite adjacent to the allotriomorphic ferrite (Fig. 6*f*) confirms the second hypothesis that the partitioning of solute prevents the formation of secondary Widmanstätten ferrite plates. A transmission electron micrograph showing the detailed morphology of the Widmanstätten ferrite plates, which can be seen to be of lenticular shape with pointed ends consistent with a displacive transformation mechanism, is shown in Fig. 6*e*.

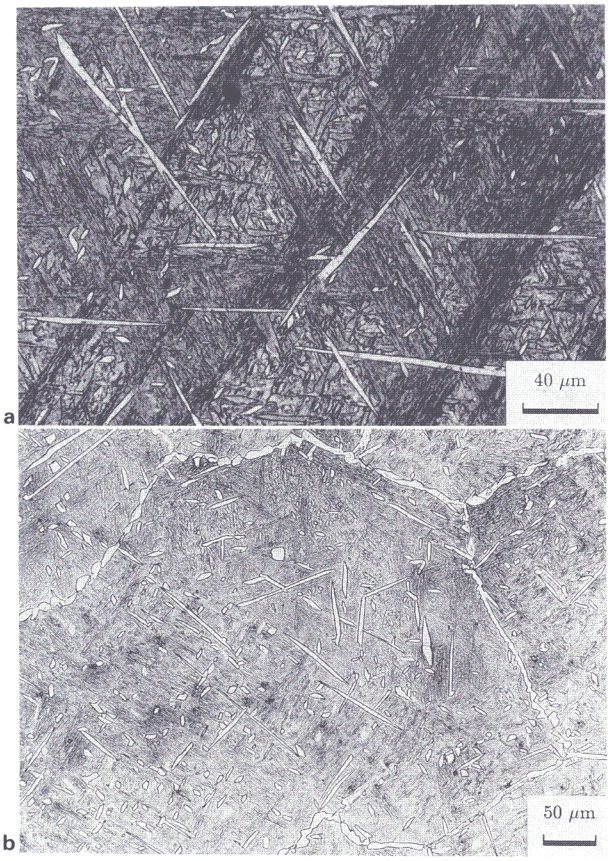

a 720°C/240 h (A2/3) and *b* 700°C/264 h (A2/6)

9 Optical micrographs of alloy A2 after isothermal transformation

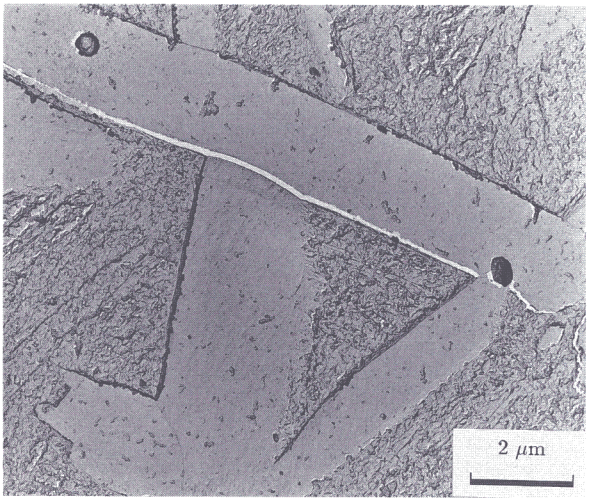

10 Carbon extraction replica image showing plates of Widmanstätten ferrite emanating from inclusion nucleation site in sample of alloy A2/6

Theory indicates that in alloy A1, Widmanstätten ferrite should form over only a very narrow temperature range, approximately 690–700°C, as illustrated in Fig. 5. Consistent with this, isothermal transformation at 680°C produced a microstructure consisting mostly of allotriomorphic ferrite and pearlite, with very few plates of Widmanstätten ferrite (Fig. 7*a*). However, after transformation at 720°C, numerous Widmanstätten ferrite plates were found (Fig. 7*b*) and, although this is in slight disagreement with the calculated transformation temperature range, examination of the 740°C sample (Fig. 7*c*) shows that the amount of Widmanstätten ferrite decreases as the temperature increases.

Metallographic measurements were carried out to confirm these observations. For ease of measurement, the time at the austenitising temperature of 1100°C was increased from 15 to 30 min (samples designated A1/10–A1/13 in Table 2). The abrupt appearance of Widmanstätten ferrite after a long incubation time is also confirmed by the histogram presented in Fig. 8*a*, which represents a quantitative analysis of the number of Widmanstätten ferrite plates counted per unit area of sample, using optical microscopy at a magnification of ×100. Consistent with the general C-shape of the Widmanstätten ferrite TTT curve (Fig. 5), both the maximum length (Fig. 8*b*) and the number density of Widmanstätten ferrite plates (Fig. 8*c*) show peaks when plotted versus the transformation temperature.

Experiments using alloy A2 revealed the same general behaviour, with the exception that the rate of reaction was always slower than that of alloy A1 (*see* Figs. 8 and 9). This is consistent with the known effect of molybdenum in retarding the reaction rate and it is notable that the retardation is evident in spite of alloy A2 having a slightly higher oxygen concentration, corresponding to a greater density of oxide particles. It is the oxides which seem to provide sites for the heterogeneous nucleation of Widmanstätten ferrite. This latter point is extremely difficult to prove on a statistical basis, because of the very low probability of observing an inclusion in a plate of ferrite,[12] but supporting evidence was nevertheless obtained using carbon extraction replicas for TEM. An example is shown in Fig. 10, in which it can be reasonably claimed that clusters of Widmanstätten ferrite plates radiate in many directions from an inclusion. Microanalysis of these inclusions extracted on the replica indicates that they are predominantly aluminium/iron/silicon rich oxides (*see* Table 4, which does not account for oxygen).

AUSTENITE GRAIN SIZE EFFECTS

The transformation start temperature W_s for austenite grain boundary nucleated Widmanstätten ferrite is known to increase with austenite grain size.[36] However, the present experiments are concerned with intragranularly nucleated ferrite, the kinetic behaviour of which should not be dependent on the austenite grain structure. To investigate this, four samples (A1/14, 15 and A2/9, 10 in Table 2) were austenitised at 1300°C rather than 1100°C. Metallographic studies confirmed that there was no noticeable difference between the two austenitising conditions (compare Fig. 11 with Fig. 7*c*). As expected from conventional hardenability theory, the greatest effect is on the grain boundary allotriomorphic ferrite reaction, which is clearly accelerated for the smaller grain sized microstructure (Fig. 7*c*).

DISSOLUTION OF WIDMANSTÄTTEN FERRITE PLATES

The Widmanstätten ferrite transformation is further from equilibrium when compared with allotriomorphic ferrite and, in the present experiments, this is manifested in its lagging behind the allotriomorphic ferrite reaction during

Table 4 Chemical compositions (wt-%) of some non-metallic inclusions found in alloy A1, obtained using energy dispersive X-ray microanalysis on transmission electron microscope

Fe	Si	Mn	Al
6	53	...	41
35	59	4	2
2	1	...	97

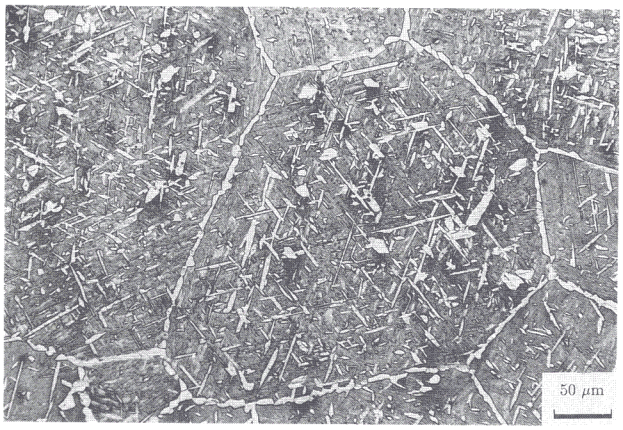

11 Microstructure of sample A1/15 after high temperature (1300°C) austenitising for 15 min, followed by isothermal transformation 740°C/264 h, then final WQ (compare with Fig. 7*c* taken from sample having smaller austenite grain size after austenitising at 1100°C for 30 min)

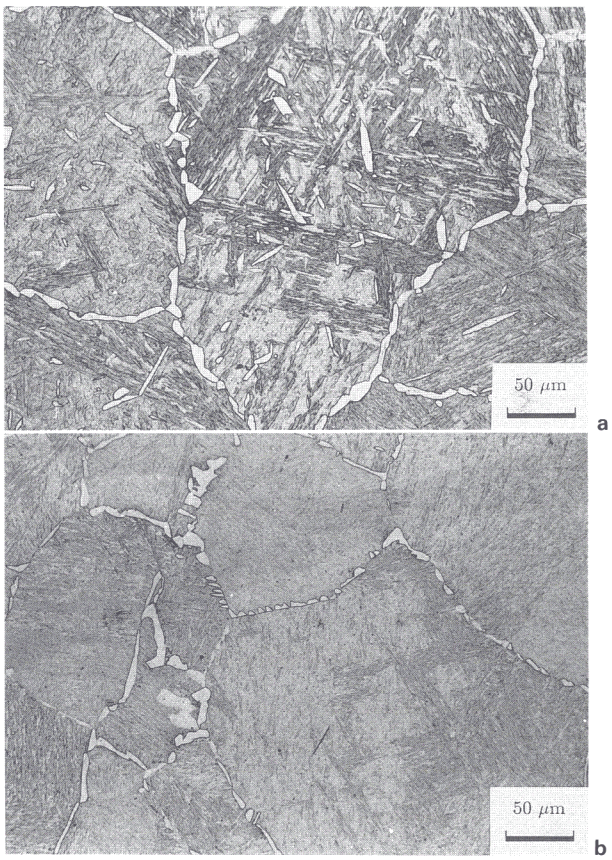

12 Samples of alloy A1 isothermally transformed at 720°C for 408 h, reheated (without cooling to below 720°C) to 800°C for *a* 60 s and *b* 60 min, then finally WQ to ambient temperature

isothermal transformation. Unlike allotriomorphic ferrite, Widmanstätten ferrite grows by a displacive mechanism and consequently has a higher stored energy; there is never any substitutional element partitioning during growth and the growth interface (plate tip) is curved, giving a further deviation from equilibrium due to the capillarity effect. Because the transformation rates in the steels used are so slow compared with the experimental conditions used, it is possible to conduct involved heat treatments without interference from unwanted reactions. The opportunity was therefore taken to ascertain whether on reheating the mixed microstructure of allotriomorphic ferrite, Widmanstätten ferrite, and austenite, the various types of ferrite would dissolve at different rates.

Any deviation from equilibrium during ferrite growth should allow it to redissolve more easily during heating, assuming the absence of any peculiar hysteresis effects associated with the tendency to equilibrate after ferrite formation. It can be seen from Fig. 8*b* that Widmanstätten ferrite precipitates profusely in alloy A1 when the alloy is isothermally transformed at 720°C. Consequently, samples of alloy A1 were heat treated as follows: 1100°C/30 min + 720°C/408 h + 800°C/t, WQ where t represents time at 800°C. It can be inferred from Fig. 12 that Widmanstätten ferrite begins to dissolve much more rapidly than allotriomorphic ferrite, confirming its non-equilibrium status compared with allotriomorphic ferrite.

Summary and conclusions

It was found possible to stimulate intragranular nucleation and growth of plates of Widmanstätten ferrite in some high strength steels, in spite of their high purity and low oxygen concentration $<0{\cdot}006$ wt-%. The effect was achieved by heat treatment to decorate the austenite grain surfaces with thin layers of allotriomorphic ferrite, which effectively rendered the austenite grain boundaries ineffective with respect to their usual ability to nucleate Widmanstätten ferrite heterogeneously. It appears that secondary nucleation of Widmanstätten ferrite on the austenite/allotriomorphic ferrite boundaries could not occur because the adjacent austenite was enriched with and stabilised by the solute partitioned during the growth of the allotriomorphic ferrite.

For the technique to be effective, the steel composition must be such as first to allow formation of allotriomorphic ferrite, followed by formation of Widmanstätten ferrite. This in turn means that the Widmanstätten ferrite C-curve on the TTT diagram must be shifted to longer times compared with that for allotriomorphic ferrite, at the temperature of heat treatment. The temperature range over which Widmanstätten ferrite can be obtained has been demonstrated to be consistent with a published model for the mechanism of the Widmanstätten ferrite transformation.[26] The metastability of the Widmanstätten ferrite with respect to allotriomorphic ferrite has also been demonstrated by the former being the first phase to dissolve when the microstructure was reheated to a temperature where austenite growth becomes possible.

The original purpose of the work was to achieve refinement of the martensitic microstructure by subdividing the austenite grains into finer blocks. Although that aim has been achieved, the prolonged heat treatments utilised are impractical. Nevertheless, the theoretical insight gained from the experiments forms a basis for further work in the design of alloys that can transform to the desired microstructure during continuous cooling heat treatment. The mechanical properties of the mixed microstructure of intragranularly nucleated Widmanstätten ferrite and martensite also have yet to be characterised.

Acknowledgments

The authors are grateful to Professor C. J. Humphreys for the provision of laboratory facilities at the University of Cambridge. The contribution of one of the authors (HKDHB) to this work was carried out under the auspices of the Atomic Arrangements: Design and Control project

which is a collaboration between the University of Cambridge and the Research and Development Corporation of Japan (JRDC). The work of the other author (AA) was funded by the Government of Pakistan and Dr A. Q. Khan Research Laboratories, Pakistan.

References

1. F. B. PICKERING: 'Transformation and hardenability in steels', 109; 1967, Ann Arbor, Climax Molybdenum.
2. R. S. CHANDEL, R. F. ORR, J. A. GIANETTO, J. T. McGRATH, B. M. PATCHETT, and A. C. BICKNELL: 'The microstructure and mechanical properties of narrow gap welds in 2·25Cr1Mo steel', Report ERP/PMRL 85–16(OP–J), Physical Metallurgy Research Laboratories, CANMET, Energy, Mines and Resources Canada, Ottawa, ON, Canada, 1985.
3. J. P. NAYLOR and P. R. KRAHE: *Metall. Trans.*, 1974, **5**, 1699–1701.
4. Y. OHMORI, H. OHTANI, and T. KUNITAKE: *Met. Sci.*, 1974, **8**, 357–366.
5. P. BROZZO, G. BUZZICHELLI, A. MASCANZONI, and M. MIRABILE: *Met. Sci.*, 1977, **11**, 123–129.
6. S. MATSUDA, T. INOUE, and M. OGASASWARA: *Trans. Jpn Inst. Met.*, 1968, **9**, 343.
7. S. MATSUDA, T. INOUE, and M. OGASASWARA: *Trans. Iron Steel Inst. Jpn*, 1972, **12**, 325.
8. W. F. SAVAGE and A. H. AARONSON: *Weld. J.*, 1966, **45**, 85–90.
9. P. RODRIGUES and J. H. ROGERSON: 'Low carbon structural steels for the eighties', 41–50; 1977, London, The Institute of Metals.
10. J. G. GARLAND amd P. R. KIRKWOOD: *Met. Const.*, 1975, **7**, 5–6.
11. J. BILLY, T. JOHANSON, B. LOBERG, and K. E. EASTERLING: *Met. Technol.*, 1980, **14**, 67–78.
12. H. K. D. H. BHADESHIA: 'Recent trends in welding science and technology', (ed. S. A. David and J. M. Vitek), 189–198; 1989, Materials Park, OH, ASM International.
13. M. IMAGUMBAI, R. CHIJIIWA, N. AIKAWA, M. NAGUMO, H. HOMMA, S. MATSUDA, and H. HIMURA: 'HSLA steels: metallurgy and applications', (ed. J. M. Gray, *et al.*), 557–566; 1985, Materials Park, OH, ASM International.
14. K. YAMAMOTO, S. MATSUDA, T. HAZE, R. CHIJIIWA, and H. MIMURA: in Proc. 'Residual and unspecified elements in steel' 1–24; 1987, Materials Park, OH, ASM International.
15. R. CHIJIIWA, H. TAMEHIRO, M. HIRAI, H. MATSUDA, and H. MIMURA: 'Offshore mechanics and Arctic engineering conference (OMAE)', Houston, TX, November 1988, pp. 1–8.
16. K. NISHIOKA and H. TAMEHIRO: 'Microalloying '88: International symposium on applications of HSLA steel', Chicago, IL, Sept. 1988, pp. 1–9.
17. H. K. D. H. BHADESHIA: *Steel Technol. Int.*, 1989, 289–294.
18. M. J. ROBERTS: *Metall. Trans.*, 1970, **1**, 3287–3294.
19. E. HORNBOGEN: *Int. Mater. Rev.*, 1989, **34**, 277–296.
20. Y. TOMITA and K. OKABAYASHI: *Metall. Trans.*, 1983, **14A**, 485–492.
21. Y. TOMITA and K. OKABAYASHI: *Metall. Trans.*, 1985, **16A**, 73–82.
22. S. S. BABU and H. K. D. H. BHADESHIA: *Mater. Sci. Technol.*, 1990, **6**, 1005–1020.
23. W. S. OWEN: *Trans. ASM*, 1954, **46**, 812–829.
24. J. GORDINE and I. CODD: *J. Iron Steel Inst.*, 1969, **207**, 461–467.
25. H. K. D. H. BHADESHIA and D. V. EDMONDS: *Acta Metall.*, 1980, **28**, 1265–1273.
26. H. K. D. H. BHADESHIA: *Acta Metall.*, 1981, **29**, 1117–1130.
27. H. K. D. H. BHADESHIA: *Met. Sci.*, 1981, **15**, 175–177.
28. H. K. D. H. BHADESHIA: *Met. Sci.*, 1981, **15**, 178–180.
29. H. K. D. H. BHADESHIA and L.-E. SVENSSON: *J. Mater. Sci.*, 1989, **24**, 3180–3188.
30. G. B. OLSON and M. COHEN: 'Dislocations in solids', (ed. F. R. N. Nabarro), Vol. 7, 297; 1986, Amsterdam, Elsevier.
31. R. A. RICKS, P. R. HOWELL, and G. S. BARRITTE: *J. Mater. Sci.*, 1982, **17**, 732–740.
32. A. CROSKY, P. G. McDOUGALL, and J. S. BOWLES: *Acta Metall.*, 1980, **28**, 1495–1504.
33. A. D. KING and T. BELL: *Metall. Trans.*, 1975, **6A**, 1419–1429.
34. P. L. RYDER and W. PITSCH: *Acta Metall.*, 1966, **14**, 1437–1448.
35. S. S. BABU and H. K. D. H. BHADESHIA: *Mater. Sci. Eng. A*, 1991, **A142**, 209–220.
36. P. R. KRAHE, K. R. KINSMAN, and H. I. AARONSON: *Acta Metall.*, 1972, **20**, 1109–1121.